

BEHAVIOUR OF TRAILING VORTICES IN THE VICINITY OF THE GROUND

G. Pailhas, X. de Saint Victor, Y. Touvet

ONERA/DMAE, Department of Modelling for Aerodynamics and Energetics, Toulouse, FRANCE

ABSTRACT

The aim of this experimental study is to analyze the mean velocity field and the turbulence occurring in the core of counter-rotating vortex pair in the vicinity of the ground. This experiment constitutes the second stage of a previous one the objective of which was to give a general view of a vortex pair close to the wall ; it has been conducted in the THALES water tunnel fitted with a moving belt on the test section floor. In this way, the simulation of ground effect has been undertaken.

A three-dimensional component laser Doppler Anemometer has been used to measure the three components of the velocity and every component of the Reynolds stress tensor in an YOZ plane perpendicular to the direction of the flow.

Measurements in various crosswise planes have been made in sufficiently refined grids allowing a precise description of the vortex flow. The high density of data points obtained in this experiment makes possible the analysis of vorticity and associated circulation fields. It was observed that the axial vorticity was distributed into concentric paths at the first streamwise locations ; farther downstream, a strong deformation of these iso-contour lines seems to be connected to the movement of the vortex centres when approaching the ground. Another main feature in the evolution of the vortex concerns the turbulence in the core ; its constant level is notable whatever the measurement station in the streamwise direction considered. Values of $k^{1/2}/U_0$ as high as 15% indicates that a part of the velocity fluctuations comes probably from the wandering of the vortices. Information, as the orientation of the main shear stress axis in the core, have been gained by investigating contours plots of the joint probability density functions relating to transverse velocity fluctuations and their corresponding correlations. Laser sheet visualisations have been performed to identify the instabilities present in vortex core.

A calculation code which solves the Navier-Stokes equations written in their steady three dimensional form has been applied to the counter rotating vortices for the afore-mentioned experimental conditions. Calculations start from the experimental data obtained at the first measurement station. The calculations are carried out taking into account a lower boundary moving at the same velocity as the flow.

1. INTRODUCTION

The presence of trailing vortices in wakes of aircraft issued from wing or flat tips is an important problem particularly during the approach to an airport. The knowledge of the physics of the vortex and of its evolution is linked to current concerns as drag reduction, airport traffic or aeronautic pollution. During landing or take off phases, trailing vortices propagate in the vicinity of the ground. So, to improve the safety by avoiding any encounter between vortices and following aircraft, standard separations between aircraft have been created. Due to a constant traffic growth, various studies have been undertaken in order to optimize these safety separations.

An experimental study has been launched in the THALES water tunnel of ONERA fitted with a moving belt on the test section floor. In this way, the simulation of ground effect has been undertaken. The vortex pair is generated by two rectangular wings located horizontally in the test section, facing each other and separated a quarter of chord apart from one another. The path of the vortex center in ground effect has been analyzed as well as the evolution of the vortices through their mean and turbulent velocity fields. Measurements have been made with a three-dimensional components laser Doppler Anemometer in various crosswise planes in sufficiently refined grids allowing a precise description of the vortex flow.

Results concerning turbulence and instabilities in vortex core are mainly discussed in the present paper.

A Navier-Stokes solver has been applied to the counter rotating vortices for the aforementioned experimental conditions.

2. EXPERIMENTAL SET-UP

THALES Water Tunnel.

The experimental study has been carried out in the T.H.A.L.E.S. water tunnel; it is essentially of a recirculating type and resembles a conventional closed circuit wind tunnel. Water runs into the loop by the way of a motor driving a simple impeller situated in the low corner of the tunnel. Water velocities in the test section are continuously variable from 0.1ms^{-1} to 7.0ms^{-1} . The velocity variations at the test section entrance are lower than 1% of the mean velocity, whatever the value of the free-stream velocity, after an effective contraction ratio of 10:1.

The horizontal test section is 0.5 m large, 0.3 m high and 3 m long; the four walls are made of glass or plexiglas, which provides good optical access for flow visualization.

A heat exchanger, located in the lower part of the circuit, allows the temperature of the water to vary. The pressure inside the loop can be adjusted in order to avoid eventual cavitation problems. The main parameters (velocity, pressure and temperature) governing the flow are constantly controlled and adjusted by a micro computer via an automaton.

The tunnel is fitted with a displacement mechanism controlled by a computer allowing linear displacements of the optical probe of the Laser Doppler Anemometry system and measurements at any location in the test section volume. The traversing unit contains step by step motors which permit remote movement of the probe in the streamwise and vertical directions. The probe location is determined with the aid of encoders allowing position resolution of 0.01 mm per encoder pulse.

The test section floor has been removed and replaced by a moving belt in order to simulate the ground effect. The moving belt is running at the same velocity that the water in the test section.

Titre:
(NACA.eps)
Auteur:
Adobe Illustrator(r) 6.0
Aperçu:
Cette image EPS n'a pas été enregistrée
avec un aperçu intégré.
Commentaires:
Cette image EPS peut être imprimée sur une
imprimante PostScript mais pas sur
un autre type d'imprimante.

Figure 1 – Schematic of the experimental set-up

Model.

The vortex pair is generated using two identical half-wings located horizontally in the test section, facing each other and separated a quarter of chord apart from one another (figure 1). Both have a rectangular planform corresponding to a NACA0015 section with a chord length c of 0.10m and a half-span of 0.225 m.

The half-wings are located at one chord distance from the floor with a negative incidence angle of 5.45° . Both are equipped at their tip with a 0.1 mm calibrated injector through which helium bubbles are generated for visualizations.

This experimental set-up is identical to that described by Devenport et al. [2].

The sketch (figure 1) shows the system of coordinates used for the present study: the X-axis is along the mean flow direction, Y is parallel to the airfoil trailing edge and Z is in the transverse direction, perpendicular to both X- and Y-axis. X=0 refers to the airfoil leading edge, Y=0 corresponds to the test section centre-line.

Test conditions.

The experiments are conducted for a constant tunnel water speed of 2 ms^{-1} and a practically constant water temperature of 293K. This leads to a free stream Reynolds number based on the model chord length of about 200,000.

Transition is tripped on the lower and upper sides of the model by a 0.1 mm diameter trip wire stuck parallel to the leading edge, at about 3% of chord length.

Measurement technique.

In the present experimental study, measurements include essentially flow scrutinizing in the core of one of the two vortices through Laser Doppler Anemometry system.

A three-dimensional component Laser Doppler Anemometer is used to measure the magnitude and direction of the velocity vector and elements of the Reynolds stress tensor in the Y-Z plane. The L.D.A. system uses a coherent argon ion laser operating with a power of about 1.5W.

The light beam from the laser is split into three components: one green ($\lambda=514 \text{ nm}$), one blue ($\lambda=488 \text{ nm}$) and the other violet ($\lambda=476 \text{ nm}$). Each color component of the laser is further split into two beams; one relating to each color passed through a Bragg cell containing a 40MHz transducer.

The L.D.A. system is used in a backward scattering mode. The two optic heads are arranged in the YOZ plane: the four beams probe is located in such a way that its axis is perpendicular to the upper wall of the test section whereas the two violet beams probe is perpendicular to the lateral wall and consequently perpendicular to the axis of the former probe. So, the probes produce convergent beams that enter the water tunnel through one of its upper and lateral glass wall respectively. The front lens of the optical system has a focal length of 400 mm in air and the laser beam pairs are focused down to a diameter of about $180 \mu\text{m}$ at the measuring point which has a length of 4 mm.

The seeding of the flow is made by means of iridium powder (particles with a mean size of $2 \mu\text{m}$) added to the circulating water in the tunnel. Light scattered by particles travelling through the intersection volume is collected by the probe's lens and then focuses into a receiver fiber optic cable which carries it to the output which feeds the light to the photomultiplier.

Data acquisition is done by means of Burst Spectrum Analyzers used in master-master configuration; frequencies and arrival times of particles in the B.S.A. output buffers are transferred to a Macintosh computer. A post processing of these data information validates the measured values related to the three B.S.A. counters for which the arrival time differences are within a certain preset coincidence time window.

Positioning of the measuring point in the X, Y and Z directions is done by steps motors under computer control. Time for traversing is used for displaying mean value, standard deviation and correlation of the three velocity components at the point measured just before. Mean and fluctuating quantities are obtained from average over 2000 samples and standard statistic treatment, respectively.

The task of the LABVIEW data acquisition system is also to provide continually on a graphical display the main elements of the data processing (instantaneous velocity signals, velocity histograms, arrival times comparison, number of validated data) allowing the permanent control of the validity of the L.D.A. measurements.

Measurement uncertainties, mainly attributable to the optical system, include the uncertainty in the measurement of the cross beam angles of laser beam orientation and in the misalignment of laser beams at probe volume. If so, the fringe pattern is either diverging or contracting along the optical axis and its spacing variation yields different signals frequencies for the same velocity depending where the particle passes through the sample volume. Bias errors in instantaneous velocity component may also arise as a result of a velocity lag between particles and flow, noise in signals... and so forth.

A systematic analysis of the bias errors has not been performed.

3. ANALYSIS AND RESULTS

Measurements are performed in various YOZ sections perpendicular to the streamwise direction. In fact, four cross-section planes have been chosen: the first two planes are located in the downward region of the vortices ($X=500$ mm and $X=1000$ mm) whereas the last two correspond to the region where the vortices are in the vicinity of the ground ($X=1200$ mm and $X=1500$ mm).

In order to get a precise description of mean and turbulent velocity fields, measurements in various crosswise planes have been made in sufficiently refined grid (1×1 mm²) composed of about thousand points in the vortex core; only the right vortex has been probed in such a way.

3.1 Mean velocity field

Figure 2 illustrates the flow field in terms of contours of axial and transverse velocities at the first measurement station. It can be seen that the mean velocities levels are nearly arranged in perfect concentric paths. Then, a precise location of the region where the transverse velocities exhibit a sign reversal can be easily done.

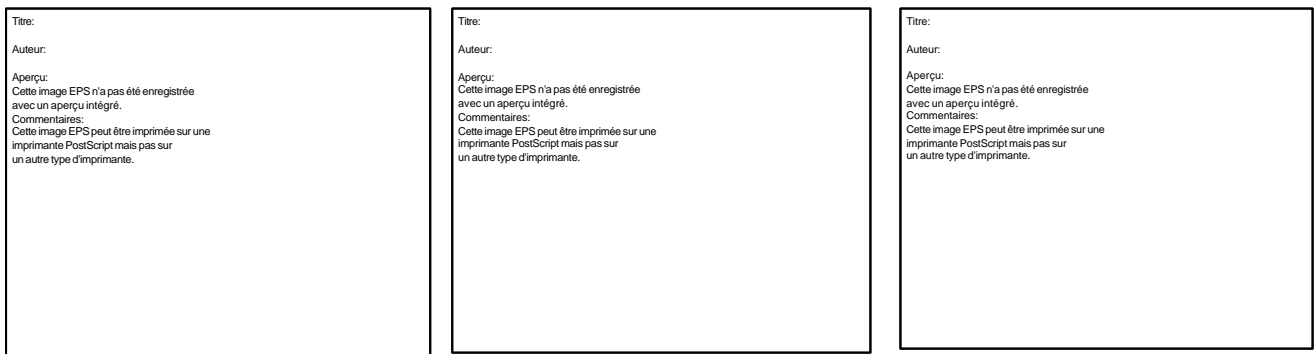


Figure 2 – Mean velocity field ($X=500$ mm)

Farther downstream, when the vortex is nearby the ground ($X=1200$ mm), the iso-contours of the three components of the velocity are clearly distorted (figure 3).

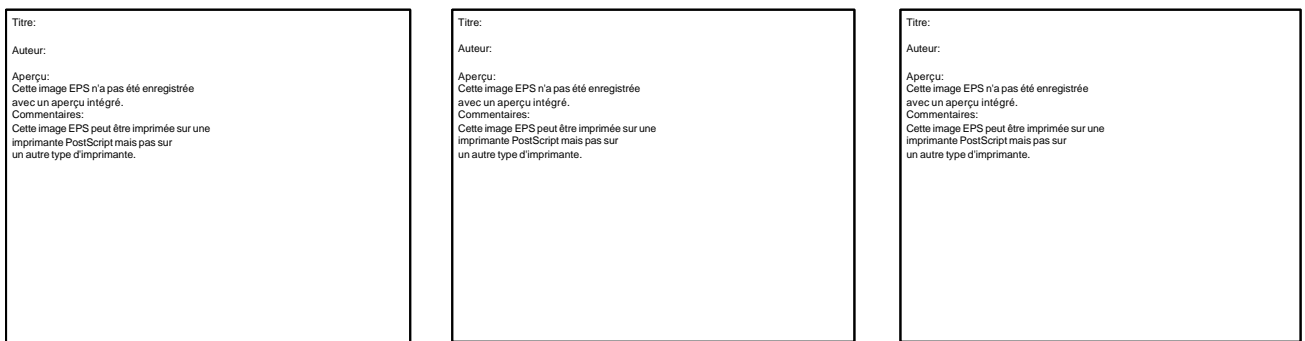


Figure 3 – Mean velocity field ($X=1200$ mm)

This distortion does not basically correspond to a disorganization of mean flow inside the vortex but, for a most part, to a bias in the measurement procedure due to the wandering motion of the vortex.

The streamwise velocity at the centre of the vortex is generally lower than in the free stream: the axial velocity defect is about 10%.

Figure 4 gives the evolution of the tangential velocity profiles along the horizontal axis of the vortex. The measured decay of V_θ does not appear as great as it would be expected from viscous effects or strength attenuation in time.



Figure 4 – Tangential velocity

The high density of data points obtained in this experiment allowed to estimate the streamwise component of the vorticity.

The contours of mean axial vorticity $w_x d / U_0$ at the first investigated station (X=500 mm) give a perfect picture of vortex roll-up. They show that vorticity is almost concentrated near the centre of the vortex; the vorticity initiated in the core at the time of formation process keeps itself nearly intact as it could be observed in a previous study [4]. Downstream (X=1200 mm), the strong distortion of the iso-contours lines leads to a bipolar structure of the vorticity; the unsteady nature of the flow is thus once again apparent.



Figure 5 – Contours of mean axial vorticity

3.2 Turbulent field

The vortex core can be assimilated to an area of homogenous flow within which turbulence would be confined and submitted to rotation effect. In the near field of the wake (where the vortices are going down towards the ground) the longitudinal fluctuation of the velocity exhibits a maximum level in the core; the quantity $\sqrt{u'^2} / U_0$ is nearby 5%. The transverse fluctuations of the velocity $\sqrt{v'^2} / U_0$ and $\sqrt{w'^2} / U_0$ present a higher level in maximum of intensity (15%)

occurring near the centre of the vortex. When the vortex approaches the ground ($X=1000$ mm) the concentric arrangement of iso- u' lines is broken down. Farther ($X=1200$ mm and $X=1500$ mm) the turbulence seems to become disorganized probably by reason of the presence of the ground.

The iso-contours of the kinetic energy k ($2k = \overline{u'^2} + \overline{v'^2} + \overline{w'^2}$) at the different measurement stations (figure 6) point out that the turbulence inside the core does not suffer of considerable modifications as regards its level and its distribution; the maximum value of $k^{1/2} / U_0$ (0.15 at the first station) remains roughly constant with X .

The refined grid adopted for probing the vortex provides a spatial resolution adequate for the evaluation of the correlation terms of Reynolds stress tensor ($\overline{u'v'}$, $\overline{u'w'}$ and $\overline{v'w'}$) in the YOZ cross-section. It can be noted that in the free-stream aligned Cartesian coordinate system, the correlation terms $\overline{u'v'}$ and $\overline{u'w'}$ correspond to the components of the shear stress vector in the YOZ plane. Their weak level combined with the experimental noise due to the vortex instability make difficult their interpretation. These correlation terms exhibit a sign reversal in the vicinity of the vortex centre and their dissymmetry is more or less important depending on the X station.

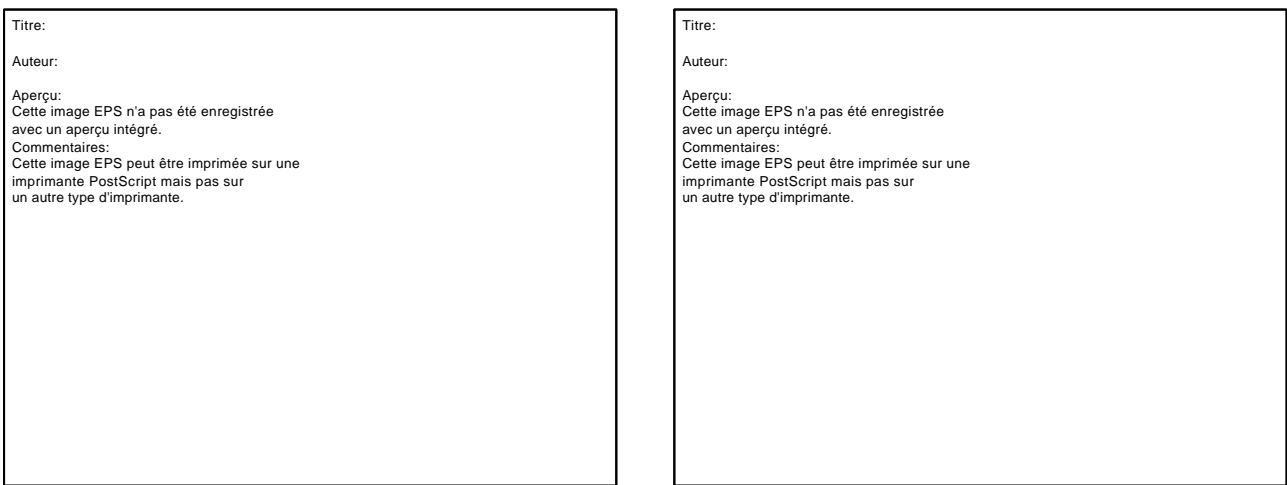


Figure 6 – Contours of turbulent kinetic energy

Information on the joint correlation terms ($\overline{u'v'}$ and $\overline{u'w'}$) contributing to shear effect in a cross-section of the vortex can be gained by investigating contour plots of the corresponding joint probability density function (figure 7). At the first measurement station, the shear stress (contained in YOZ plane) is mainly aligned with a 45° direction reminding that of Crow instability [1]. At $X=1000$ mm, the iso probability contours alter in such a way the principal orientation observed at the previous station disappears. At the last measurement stations ($X=1200$ mm and $X=1500$ mm) the $\overline{u'w'}$ correlation becomes large compared to $\overline{u'v'}$; the iso-probability contours are then aligned with the OZ direction.

All these measurements indicate a substantial change in the turbulence structure as the vortex approaches the ground.

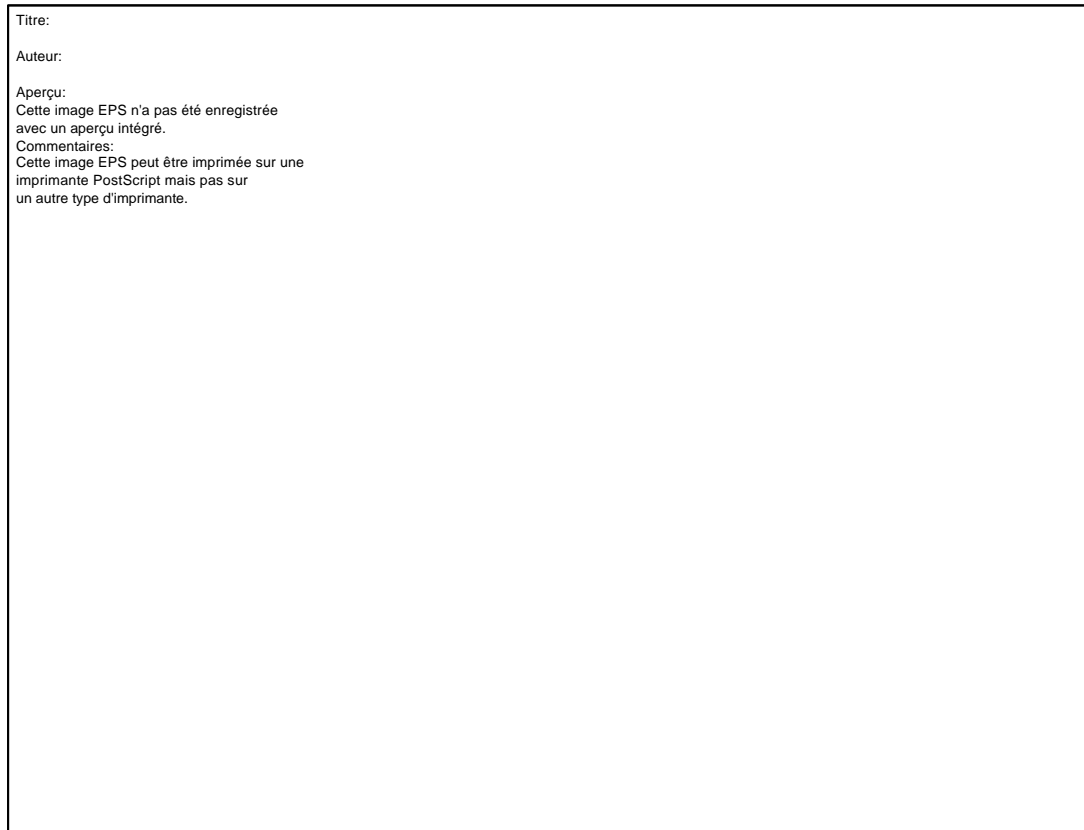


Figure 7 – $u'v'-u'w'$ joint probability density function

3.3 Vortex instability

Vortex flows are typically three-dimensional and highly unsteady. Several instability mechanisms result of interactions between counter-rotating vortices generated by lifting surfaces. In a general way, two kinds of instabilities can be identified: the long-wave instability which was first studied theoretically by Crow [1] and the short-wave instability known as Widnall instability [6]. From Crow's analysis it can be estimated that the most-amplified wavelength is about 8 times the vortex spacing. Widnall theory predicts the development of perturbation the wavelength of which is of the order of one core diameter.

Crow instability found expression in a periodic variation of the distance separating the two vortices. In regions in which the vortices approach (under Crow instability effect) Widnall instability develops more rapidly than everywhere else. So, Widnall instability which develops in a no regular way is difficult to measure. Moreover, vortices "wander" in space what leads the core location to vary erratically in time.

Flow visualizations have been undertaken in order to give prominence to unsteady phenomenon. Helium microbubbles are injected through a calibrated hole at the tip of each rectangular wing. Bubbles used as flows markers are driven into the core and permit the instantaneous core location to be identified.

By laser sheet illumination of the flow in YOZ planes, the unsteadiness of the core vortex has been clearly pointed out. About 5000 images of the flow in the scrutinized plane are recorded by a camera and stored on a computer. In order to provide an optimal information of the instantaneous location of the vortex core an adapted image processing technique has been used.

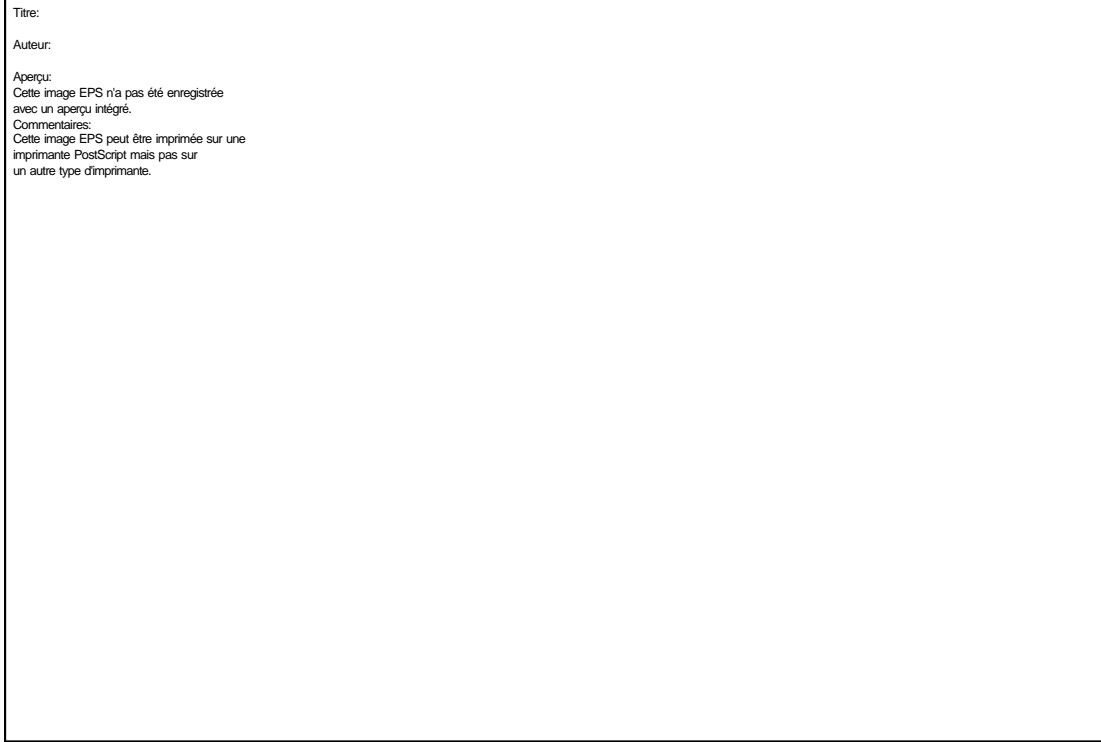


Figure 8 – Joint probability contours of Y-Z core locations

The image processing results in various scrutinized planes are given in figure 8 where the contours of the joint probability density function relating to Y-Z coordinates of the core location are plotted. At the first measurement station, the orientation of the probability contours along a 50° direction relating to OY axis is noticeable. This direction is not far distant from that corresponding to the Crow instability amplification. Farther downstream, when the vortex is in the vicinity of the ground, the probability contours show a trend towards a direction parallel to the OY axis. The vortex instability corresponds to a shifting of the vortex core in the region of its radius.

4. NUMERICAL INVESTIGATION

With the hypotheses of incompressibility and Newtonian fluid, the Navier-Stokes equations can be written for a steady three-dimensional flow:

$$\text{div}(\underline{U}) = 0$$

$$\mathbf{r} \text{div}(\underline{U} \otimes \underline{U}) = -\text{grad}P + \mathbf{m}\Delta \underline{U}$$

where P is the static pressure of the flow and \underline{U} the velocity vector of the fluid particles.

The velocity u_c and the distance l_c are selected as characteristic values.

For a pair of vortices, u_c is the velocity of descent of the pair of vortices and l_c is the distance between the two vortices.

The associated Reynolds number will be: $Re = \frac{u_c l_c}{\mathbf{n}}$

The flow, that we plan to model, is made up of two contra-rotating vortices convected by the external flow at a given velocity U_0 [5].

The evolution of the vortices depends only on the upwind stations and there is no information coming from downstream (as long as obstacles are not met). Along the axis of propagation of the vortex the behaviour of the Navier-Stokes equations must be parabolic. So, the terms of diffusion concerning the preferential direction of the flow will be eliminated in a first step.

The equations can be written:

$$\frac{\partial u}{\partial x} + \frac{\partial v}{\partial y} + \frac{\partial w}{\partial z} = 0$$

$$u \frac{\partial u}{\partial x} + v \frac{\partial u}{\partial y} + w \frac{\partial u}{\partial z} = -\frac{\partial p}{\partial x} + \frac{1}{Re} \left(\frac{\partial^2 u}{\partial y^2} + \frac{\partial^2 u}{\partial z^2} \right)$$

$$u \frac{\partial v}{\partial x} + v \frac{\partial v}{\partial y} + w \frac{\partial v}{\partial z} = -\frac{\partial p}{\partial y} + \frac{1}{Re} \left(\frac{\partial^2 v}{\partial y^2} + \frac{\partial^2 v}{\partial z^2} \right)$$

$$u \frac{\partial w}{\partial x} + v \frac{\partial w}{\partial y} + w \frac{\partial w}{\partial z} = -\frac{\partial p}{\partial z} + \frac{1}{Re} \left(\frac{\partial^2 w}{\partial y^2} + \frac{\partial^2 w}{\partial z^2} \right)$$

The result of this simplification is that the equations are now written in a form known as semi-elliptic. Indeed, it keeps an elliptic character because of the presence of the longitudinal pressure gradient. Nevertheless, given that latter leads to compute the flow using the Navier-Stokes equations written in their parabolic form.

The simplifying assumptions will allow to use an X-marching method according to the preferential direction of the flow. The problem remains elliptic in each orthogonal plane to this direction and will be solved thanks to the SIMPLE algorithm.

In the parabolic case, one sweep will be only carried out along the preferential direction. This case corresponds to an unsteady two-dimensional “temporal axis”.

In the semi-elliptic case, information coming from downstream will be taken into account through the longitudinal pressure gradient. As the pressure gradient is unknown, several sweeps according to the preferential direction are carried out and the pressure field is stored on all the field of calculation. The stability of the solution is ensured by a downward discretization of the pressure gradient.

A grid constituted by 100 × 180 × 90 points is used. Two squares with 50 × 50 points are defined including the two main vortices.

The vortices are observed from the abscissa x=0.5m to 1.5m downstream from the wings.

The calculations are carried out taking into account a lower boundary moving at the same velocity as the flow ($U_0=2\text{ms}^{-1}$). In the experiments the moving belt is 0.4m large i.e. 80% of the width of the tunnel whereas all the boundary is moving in the numerical simulation.

The studied phenomenon is located in the central part of the test section such that this approximation does not disturb the results. The side walls and the upper wall are motionless. The development of the boundary layers on these surfaces is taken into account in the calculations.

The choice of the number of grid points is guided by the wish to have a reasonable calculation time. The longitudinal distance between two consecutive planes is then imposed by the length of the calculation domain.

Calculation start from the experimental data obtained at x=0.5m (figure 9).

By means of the longitudinal and crosswise iso-velocities, the figures 10 and 11 present respectively the experimental and numerical results. A good agreement for the crosswise velocity v is observed. On the other hand, clear differences appear between the contours related to the longitudinal velocity u. It appears an overshoot of velocity ($u > U_0$) surrounding the two main vortices. This overshoot is not found experimentally.

The figure 12 shows a good agreement on the velocity v when plotting along a vertical section of each vortex. In the same figure, but now performing an horizontal section of the cores, the evolution of the longitudinal velocity u is shown. The two cores are easily located by the minima of this component of the velocity.

The obtained result shows a reduction of the deficit of the velocity which is faster than for the measured deficit. At the outside of the cores, the overshoot already mentioned is noticed.

Watching more attentively at figure 10 it can be seen a deficit of velocity close to the wall which leads to assume the existence of a longitudinal boundary layer.

To explain this, it is assumed that the floor is not moving at exactly the same velocity as the flow.

As the calculated velocities are about 5% bigger than the flow velocity U_0 , the lower boundary is slowed down by 5%.

The obtained results are summarized in the figures 13 and 14.

We notice the disappearance of the overshoots of velocity near the wall and around the vortices.

Titre:
Auteur:
TECPLOT
Aperçu:
Cette image EPS n'a pas été enregistrée
avec un aperçu intégré.
Commentaires:
Cette image EPS peut être imprimée sur une
imprimante PostScript mais pas sur
un autre type d'imprimante.

Figure 9 – $x=0.5m$: Longitudinal and crosswise velocity -- Experiments

Titre:
Auteur:
TECPLOT
Aperçu:
Cette image EPS n'a pas été enregistrée
avec un aperçu intégré.
Commentaires:
Cette image EPS peut être imprimée sur une
imprimante PostScript mais pas sur
un autre type d'imprimante.

Figure 10 – $x=1.0m$; Longitudinal and crosswise velocities -- Experiments

Titre:
Auteur:
TECPLOT
Aperçu:
Cette image EPS n'a pas été enregistrée
avec un aperçu intégré.
Commentaires:
Cette image EPS peut être imprimée sur une
imprimante PostScript mais pas sur
un autre type d'imprimante.

Figure 11 – $x=1.0m$; Longitudinal and crosswise velocities -- Calculations

Titre:
Auteur:
TECPLOT
Aperçu:
Cette image EPS n'a pas été enregistrée
avec un aperçu intégré.
Commentaires:
Cette image EPS peut être imprimée sur une
imprimante PostScript mais pas sur
un autre type d'imprimante.

Figure 12 – $x=1.0 m$; Velocity profiles -- Experiments-calculations



Figure 13 – $x=1.0m$; Longitudinal and crosswise velocities -- new calculations

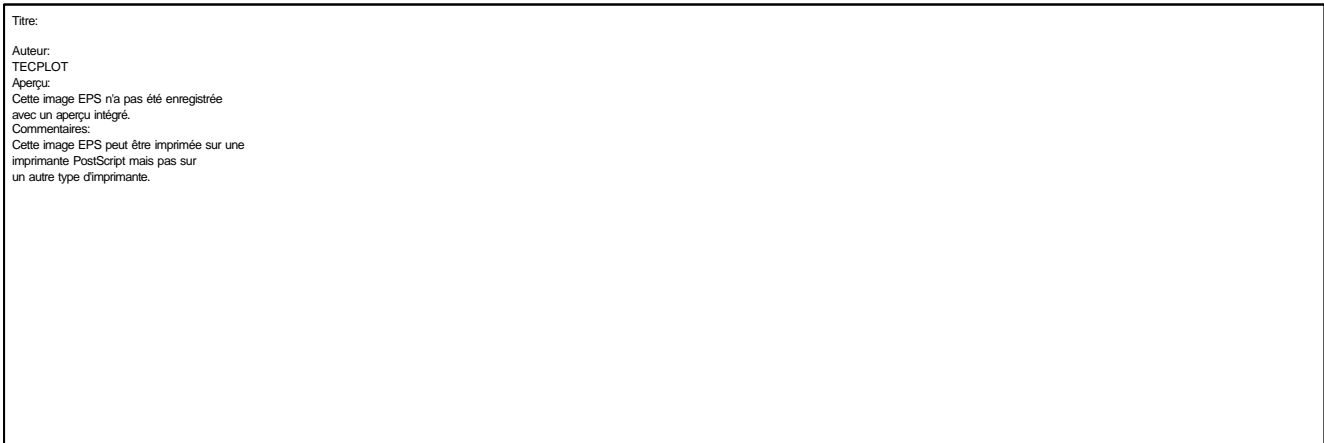


Figure 14 – $x=1.0m$: Velocity profiles -- Experiments- new calculations

Examining the longitudinal velocity profiles clearly confirms that observation (figure 14). Moreover the deficit of axial velocity in the core of the vortices is more important when the lower wall is slowed down. However these velocities remain higher than the measured ones.

A second effect of the slowdown can be seen with the profile of the vertical velocity. It can be noticed that the altitudes of the vortices are less than those obtained when the moving belt was not slowed down and that the vortices descend faster.

The formation of the secondary vortices is delayed so the rebound will occur later. In spite of these differences of position, it is noticed that the decrease of the vortices is almost the same in the two configurations. It follows the Lamb-Oseen's law.

5. CONCLUSION

An experimental study has been performed to examine the ground effect on the behavior of trailing vortices. The vortex pair were generated by two rectangular wings facing each other and separated a quarter of chord apart from one another.

A three dimensional component Laser Doppler Anemometer was used to analyze the path of the vortex center as well as the evolution of the vortex through its mean and turbulent velocity fields. The high density of data points obtained made possible such a detailed analysis.

It was observed that the vorticity concentrated in the vortex core at the time of formation process kept itself nearly intact; farther downstream, a bipolar structure of the vorticity seems to be linked to the unsteady nature of the flow.

The turbulence inside the core does not suffer of substantial modification concerning its distribution and level with X.

The analysis of the joint probability density function of the turbulent correlation terms revealed that the shear stress mainly aligned with a 45° direction at the first measurement station was strongly affected by the presence of the ground.

Trailing vortex core unsteadiness has been clearly pointed out from flow visualizations associated to an adapted image processing technique. The orientation of the probability contours of the core locations (near the Crow direction) is strongly dependent on the distance between the vortex and the ground.

Particle image velocimetry (PIV) technique is to be used to investigate instantaneous velocity fields and provide more quantitative information for the vortex instability.

These experiments allowed to validate a calculation code solving the incompressible Navier-Stokes equations. A good agreement between measurements and calculations has been found taking into account a moving belt velocity slightly different from the measured one. The calculations have been made assuming a laminar flow. Therefore, it seems that, in this case, turbulence plays a weak role in the evolution of the phenomenon.

REFERENCES

- [1] S.C. Crow, Stability theory for a pair of trailing vortices. AIAA J.. 8 (12), 1970.
- [2] W. Devenport et al., The structure and development of a counter-rotating wing-tip vortex pair. J. Fluid Mech., vol 323,1997.
- [3] T. Leweke, H.K. Williamson, Cooperative elliptic instability of a vortex pair, J. Fluid Mech, vol 360, 1998.
- [4] G. Pailhas, Y. Touvet, Turbulence et instabilité de deux tourbillons contrarotatifs de bouts d'ailes avec le sol. AAAF, Orléans, mars 2000.
- [5] X. de Saint Victor, F. Puel, M.L. Groud, Appariement et rebond de tourbillons de sillage. AAAF, Orléans, mars 2000
- [6] S.E. Widnall, D.B. Tsai, A. Zalay, Theoretical and experimental study of the stability of a vortex pair. Aircraft wake turbulence, in Rodgers Olsen, Plenum Press, 1971.
- [7] Y. Zheng, B. R. Ramaprian, LDV measurements in the unsteady tip-vortex behind an oscillating rectangular wing, 8th Symposium on Turbulent Shear Flows, Munich, 1991.